A ~~multi-purpose~~ multipurpose lifting-line flow solver for arbitrary wind energy concepts

Emmanuel Branlard[1], Ian Brownstein [2], Benjamin Strom [2], Jason Jonkman [1], Scott Dana [1], and Edward Ian Baring-Gould [1]

[1]National Renewable Energy Laboratory, Golden, CO, USA
[2]XFlow Energy, Seattle, WA, USA

Correspondence: E. Branlard (emmanuel.branlard@nrel.gov)

Abstract. In this work, we extend the AeroDyn module of OpenFAST to support arbitrary collections of wings, rotors, and towers. The new standalone AeroDyn driver supports arbitrary motions of the lifting surfaces and complex turbulent inflows. Aerodynamics and inflow are assembled into one module that can be readily coupled with an elastic solver. We describe the features and updates necessary for the implementation of the new AeroDyn driver. We present different case studies of the driver to illustrate its application to concepts such as multirotors, kites, or vertical-axis wind turbines. We perform verification and validation of some of the new features using the following test cases: elliptical wings, horizontal-axis wind turbines, and 2D and 3D vertical-axis wind turbines. The wind turbine simulations are compared to existing tools and field measurements. We use this opportunity to describe some limitations of current models and to highlight areas that we think should be the focus of future research in wind turbine aerodynamics.

1 Introduction

~~Horizontal axis~~ Horizontal-axis wind turbines (~~HAWT~~HAWTs) have been the ~~main-stream~~ mainstream focus of the wind energy community in the past few decades, and most aerodynamic tools ~~have been~~ are centered around such a concept. ~~This is, for instance,~~ For example, this is the case for the ~~multi-physics~~ multiphysics solver OpenFAST (OpenFAST, 2021) developed by the National Renewable Energy Laboratory. The OpenFAST solver ~~has been dedicated to HAWT and cannot~~is dedicated to HAWTs and cannot[1] study other wind energy concepts~~such as: vertical axis~~ , such as vertical-axis wind turbines (~~VAWT~~VAWTs), kites, airborne wind energy concepts, and arbitrary assemblies of rotors and blades/wings. This article attempts to bridge this gap by focusing on ~~adding~~ new aerodynamic functionalities to the aerodynamic model of OpenFAST, named AeroDyn. This first step can ~~later be followed~~ be followed later by extending the structural dynamics modules to accommodate these different concepts.

The most common method for the study of a HAWT is the blade element momentum (BEM) method (Glauert, 1935). The method cannot be applied to other concepts, though it inspired the development of streamtube models for ~~vertical axis turbines (De Vries, 1979)~~VAWTs (Strickland, 1975; De Vries, 1979; Paraschivoiu and Delclaux, 1983). General purpose com-

[1]Airborne wind energy kites have been modeled in OpenFAST with the extension ~~to OpenFAST~~ known as KiteFAST (Jonkman, 2021)

putational fluid dynamics (CFD) solvers are commercially available and have been applied to various wind energy concepts (Makridis and Chick, 2013; Folkersma et al., 2017; Rezaeiha et al., 2017). Their use by the wind energy community is still limited, and dedicated solvers are typically preferred. Such solvers (e.g., Ellipsys (Sørensen, 1995), FLOWer (Weihing et al., 2018), and ExaWind (Sprague et al., 2020)) have generic grid-based implementations, but they have been primarily applied to ~~HAWT~~HAWTs. However, simulations of alternative wind energy concepts using these solvers are emerging in the literature (Bangga et al., 2020). CFD applications with arbitrary motions are still challenging and not readily available. Vorticity-based methods have long been considered ~~as~~ the intermediate solution between the computationally intensive CFD methods and the engineering models, such as BEM (Perez-Becker et al., 2020; Boorsma et al., 2020). Panel-based ~~methods~~ and lifting-line methods are readily applied to arbitrary assemblies of wings and rotors (Katz and Plotkin, 2001). ~~Generic~~ The open-source code QBlade Marten et al. (2013) contains a generic vorticity-based solver that has been applied to HAWTs (Saverin et al., 2018a) and VAWTs (Saverin et al., 2018b). Other generic solvers have been implemented (Grasso et al., 2011; Chatelain et al., 2013; Branlard et al., 2015; Alvarez and Ning, 2019; Boorsma et al., 2020) but ~~often not~~ not often publicly distributed.

In this work, we leverage the recent implementation of the open-source lifting-line vortex code, OLAF (cOnvecting LAgrangian Filaments), integrated in AeroDyn (Shaler et al., 2020) and present verification and validation of this tool. We extend the AeroDyn module to support arbitrary collections of wings, rotors, and towers. Assemblies of rotors can be handled with BEM or OLAF, while more complex geometries are handled with OLAF only. The existing driver for AeroDyn is also extended to support arbitrary geometries, provide functionalities to prescribe arbitrary motions to the lifting surfaces, and prescribe complex turbulent inflows. In this work, we combined the aerodynamic and inflow modules into a standalone module so that it can readily be coupled with structural solvers, paving the way for aeroelastic simulations of arbitrary wind energy concepts.

In Section 2, we describe the features of the new AeroDyn driver, the updates to the AeroDyn modules, and briefly mention the implementation. In Section 3, we present different applications of the driver and perform verification and validation of some of its features. We use this opportunity to ~~point out~~ describe some limitations of current models and highlight areas ~~which~~ that we think should be the focus of future research in wind turbine aerodynamics. We conclude our work by summarizing these research questions and providing paths for future work.

2 Features and implementation

In this section, we describe the main features of the ~~newly-implemented~~ newly implemented AeroDyn driver. The original AeroDyn driver was limited to the simulation of HAWTs, with a fixed nacelle position, and inflows limited to a power law shear profile (more advanced structural motions and wind conditions can be simulated when coupling AeroDyn within OpenFAST, including ~~aero-elastic~~ aeroelastic effects and turbulence). To ~~be able to~~ model advanced wind energy concepts, the driver was augmented to ~~be able to~~ model rotors and wings of arbitrary geometry, undergoing arbitrary rigid-body motion ~~,~~ and under arbitrary inflows. As such, the driver can be used for configurations that are not currently supported by OpenFAST. To facilitate the future coupling with a structural solver, we combined the aerodynamic and inflow modules into a new module. ~~We proceed by listing the features of the driver~~ The features of this driver include:

– **Inflow**. The wind field may be defined in three ways: ~~using~~ (1) Using a uniform power law, ~~a time varying~~ (2) using a time-varying power law (~~were~~ where both the reference velocity and the ~~power~~ power-law coefficient change with time), or (3) using any wind supported by the InflowWind module (OpenFAST, 2021)~~: uniform~~ —uniform steady wind, unsteady wind speed and direction (e.g., deterministic gusts), and turbulent wind field of various file formats.

– **Geometry**. An assembly of fixed or rotating blades/wings is called a "turbine~~".~~." The driver can have an arbitrary number of turbines. Each turbine ~~comprise of~~ comprises one optional tower and a set of blades. An example of a configuration with two turbines is shown in Figure 1. The figure defines the different frames ~~defined for each turbine: the turbine~~ used for each turbine—the turbine base frame (labeled, t), the nacelle frame (n), the hub frame (h), and the blade frames (b). The labels are used to identify the frame axes and the origins in the following~~.~~: As indicated in Figure 1, the coordinate systems must be such that the hub rotation occurs about the x_h axis, and the blade frame must be such that x_b and y_b ~~points towards~~ point toward the suction side and the trailing edge~~respectively~~, respectively, when the pitch and twist angles are zero. The turbine base and ~~the~~ tower base have distinct origins but they share the same frame. The tower top is assumed to coincide with the nacelle origin. The origins and orientations of each ~~frames are user input~~ frame are input by the user, where coordinates are given relative to the parent frame, and orientations are given using the values of three successive rotations (x-y-z Euler angle sequence) taken from the parent frame. A user switch is available to facilitate the input of generic ~~HAWTs~~ HAWT geometries. In this framework, an arbitrary wing is ~~setup~~ set up as a turbine with no rotational speed and an optional tower.

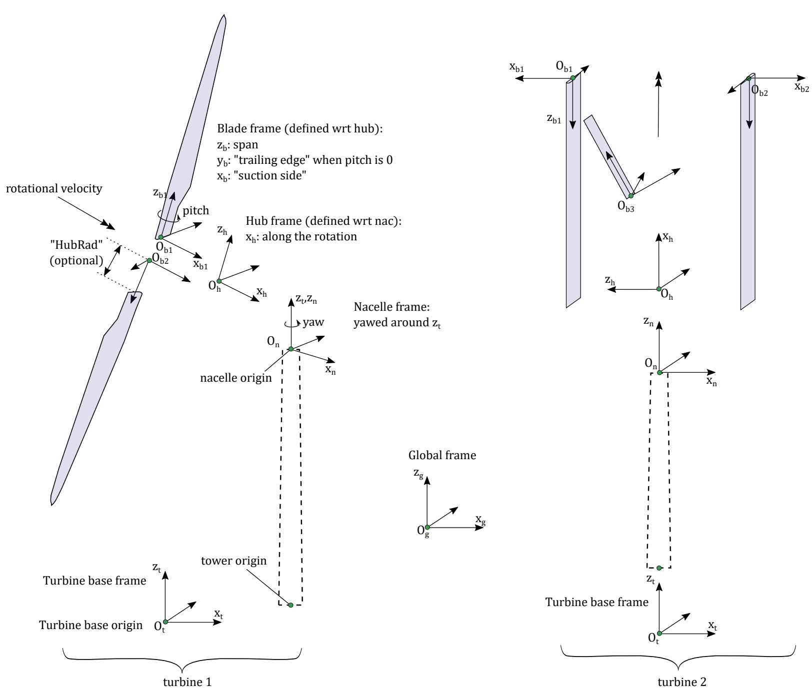

Figure 1. Definition of frames and origins for a two-turbine configuration—HAWT (left), VAWT (right).

– **Motion**. Motion inputs are provided independently for the base, nacelle, hub, and blades of each turbine. The base motion may be: fixed, sinusoidal in one of six degrees of freedom, or arbitrary. The arbitrary motion is provided using time series of: time, 3 translations, 3 successive rotations, 3 translation velocities, 3 rotational velocities, 3 translational accelerations, and 3 rotational accelerations. The nacelle yaws around the z_n axis, and the user may fix the yaw angle or provide a time series of the nacelle yaw angle, speed, and acceleration. The rotor rotates about the x_h axis, and the user may specify a constant rotational speed or a ~~time varying time~~ time-varying time series (angular position, speed, and acceleration). Blade pitching occurs around the individual z_b axes. The user can specify constant pitch or time series of pitch (position, speed, and acceleration) for each individual blade. ~~Non-rotary~~ Nonrotary wings are considered as a special case with 0 rotational speed. The different rigid-body motions are easily implemented using the mesh-mapping routines of OpenFAST, called within the AeroDyn driver.

– **Flow solver**. The driver operates with AeroDyn, and the different wake options of AeroDyn can be used to solve the flow. The options currently available are: no induction (using the geometric angle of attack)~~,~~; quasi-steady and dynamic BEM for ~~HAWT (Moriarty and Hansen, 2005; Branlard, 2017), or a~~ HAWTs (Moriarty and Hansen, 2005; Branlard, 2017) ; or the vortex wake code~~named OLAF(cOnvecting LAgrangian Filaments)~~, OLAF (Shaler et al., 2020). AeroDyn is currently being extended to support hydrokinetic turbines (including buoyancy and added mass effects)~~and future implementation~~; future implementations will include a ~~double-streamtube momentum model for vertical axis turbines~~double-streamtube-momentum model for VAWTs. Currently, BEM and OLAF cannot be used simultaneously, but such options will be considered in the future.

– **Analysis types**. Different analysis types are provided by the driver. In particular, parametric studies can be run by providing a table of combined-case analyses. ~~The reader is referred~~ Refer to the OpenFAST manual for additional details (OpenFAST, 2021).

– **Outputs**. The driver outputs time series of motion, loads, and aerodynamic variables to individual files for each turbine. Additionally, 3D visualization outputs are available for the individual bodies. When OLAF is used, Lagrangian markers and velocity/vorticity planes can be output to visualize the wake.

Changes to the AeroDyn module consisted ~~in~~ of supporting multiple rotors throughout the code, with different parameters for each rotor, and extending OLAF so that it can handle an assembly of wings with different ~~number~~ numbers of input sections. In this work, we added two dynamic stall models to ~~AeroDyn: the~~ AeroDyn—the Boeing-Vertol (BV) model (also present in CACTUS (Murray and Barone, 2011)) ~~,~~ and the dynamic stall model of Øye (Øye, 1991; Branlard, 2017). Both models are documented in the OpenFAST documentation (OpenFAST, 2021). The driver was fully rewritten to accommodate the new features and to couple with the new module that combines aerodynamic and inflow. The source code of the AeroDyn driver is open-source and available on the OpenFAST repository (OpenFAST, 2021), together with its documentation. Example input files, including some of the cases presented below, are also available and integrated as part of the OpenFAST testing framework.

3 Results: Verification, validation, and path forward

3.1 Illustrative examples

We begin the application this section by showing visual outputs from simulations done using the AeroDyn driver applied to different wind energy concepts. The vortex wake formulation (OLAF) OLAF was used for all simulations because it can be applied to arbitrary geometries and it offers an opportunity to visualize the wake. Visualizations of the wake, blades, towers, and velocity planes are given shown in Figure 2 for : an elliptical wing, a vertical axis wind turbineVAWT, a kite performing a "8-figurefigure-8," and a "quad-rotor" with multiple towers. In the quad rotor figure, the impact of the tower shadow and the wakes is observed in the velocity field. In the remaining portion of this section, we will dive into specific applications , in order look at specific applications to verify and validate the current implementation. Each investigation will point to research topics for future work on the aerodynamics of wind energy concepts. The These points will be summarized in the conclusion.

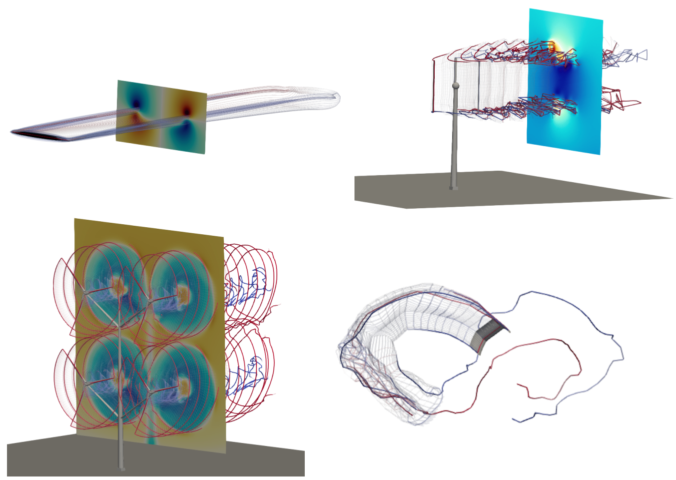

Figure 2. Example of wind energy concepts to which the AeroDyn driver may be applied: applied—(clockwise from top left) elliptical wing, vertical axis turbineVAWT, kites, and multiple rotors, kites.

3.2 Elliptical wing and HAWT—Effect of regularization

3.2.1 Elliptical wing

In this section, we use the elliptical wing test case presented by van Garrel (van Garrel, 2003) to illustrate the capability of the AeroDyn driver in studying isolated lifting lines (not necessarily rotors). The wing span wingspan is $b = 5$ m, the chord $c = c_0\sqrt{1-2y/b}$, with $c = c_0\sqrt{1-2(y/b)^2}$, where $c_0 = 1$ m, the $n+1$ panel nodes are located via a cosine distribution at the spanwise coordinates $y = b/2\cos\theta$, with θ spanning linearly from $-\pi$ to π. The control points are located between the panel nodes, according to the cosine-approximation algorithm of van Garrel. The wind speed is 1 m/s in the chordwise direction and 0.1 m/s normal to the chord, leading to a geometrical angle of attack of 5.7106 deg. The profile data is uniform along the ~~wing span~~ wingspan and set with a linear lift coefficient: $C_l(\alpha) = 2\pi\alpha$. The wake convects with the free-stream only (no rollup). ~~Three different number of panels are used~~ We use three different numbers of panels for the verification: $n = [20, 40, 80]$. ~~Baseline resultsare obtained with no~~ The baseline results, similar to van Garrel's study, are those without regularization (no "vortex core"), indicated by a zero value of the regularization parameter ϵ. ~~To illustrate~~ We demonstrate the impact of the regularization ~~, simulations for~~ by performing simulations with $n = 80$~~are shown for~~ , with a regularization parameter proportional to the chord ($\epsilon = 0.5c$) ~~and~~ or with a constant parameter ($\epsilon = 0.1$~~.~~). We use a Lamb-Oseen regularization kernel as a multiplicative factor to remove the singularity; the regularization parameter is the same for the wing and the wake and is constant throughout the wake. The lift coefficient along the span is shown in Figure 3. It was obtained using OLAF ~~,~~ coupled with the AeroDyn driver. The vortex wake results extracted from van Garrel's report are also ~~given~~ provided in the

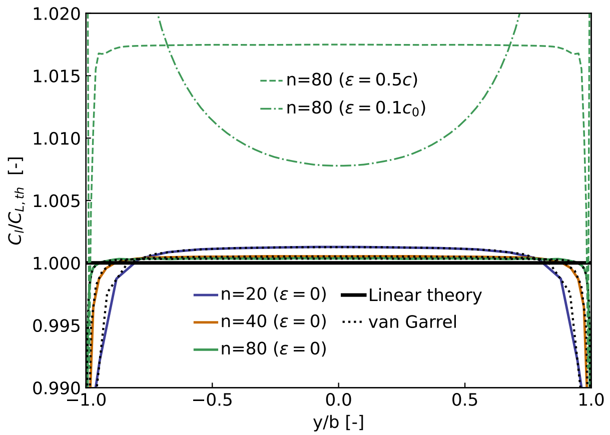

Figure 3. Lift coefficient along elliptical wing (C_l) as predicted by two similar lifting-line implementations (OLAF ~~,~~and van Garrel) and the linear lifting-line theory ($C_{L,th}$). Results for various ~~number~~ numbers of spanwise stations (n) and regularization parameters (ϵ).

figure. The strong agreement between the two vortex wake codes supports the verification of OLAF's implementation. Both lifting-line implementations are expected to rely on the same formulation. The results from AeroDyn are reported at the panel nodes and not the control point nodes of OLAF, explaining the minor differences observed ~~towards~~ toward the wing tips for $n = 20$. Under the linear and classical lifting-line approximation of Prandtl (Katz and Plotkin, 2001; Branlard, 2017), the theoretical lift coefficient for the wing is $C_{L,\text{th}} = 2\pi\alpha[1 + 2/\text{AR}]^{-1} \approx 0.47653$, where $\text{AR} = b^2/(\pi b c_0/4)$ is the wing aspect ratio. The theoretical value is indicated on the figure. The current simulation setup (cosine distribution without regularization and wake rollup) is well suited to approximate the linear theory ~~,~~but is not expected to match the results fully. To match the linear theory, linear assumptions are needed, and the wake needs to follow the chord instead of the freestream. Requirements to match the theory exactly are provided in Chapter 3 of (Branlard, 2017). The impact of the regularization is clearly observed in Figure 3, and the choice of the regularization parameter can have a drastic impact on the results.

~~A realistic simulation of an elliptical wing requires regularization to account for the~~

3.2.2 HAWT

To illustrate the impact for a HAWT, we use the Big Adaptive Rotor (Bortolotti et al., 2021) operating at a tip-speed ratio of $\lambda = 8$, with a thrust coefficient of $C_T = 0.64$, and a power coefficient of $C_P = 0.46$.

In the plot on the left of Figure 4, we show the different regularization parameter distributions used, normalized by the maximum chord of the turbine. The regularization parameter is either proportional to the chord or to the spanwise discretization (here, the spanwise discretization is constant). We plot the resulting axial and tangential induction factors along the blade on the middle and right of Figure 4. We observe that the regularization parameter influences the induction at the tip, middle, and root of the blades, where circulation gradients are the strongest. A large value of the regularization factor leads to smoother, more regular, induced velocity distributions, whereas lower values allow for more sudden changes. In this particular example, we observed (results not included here) differences in normal and tangential loads of up to 6% and 30%, respectively, within the first 40% span of the blade, and differences up to 2% and 8% toward the tip of the blade. The power and thrust coefficients vary up to 2.3% and 0.7%, respectively. Both variables tend to take larger values with increased values of the regularization parameter.

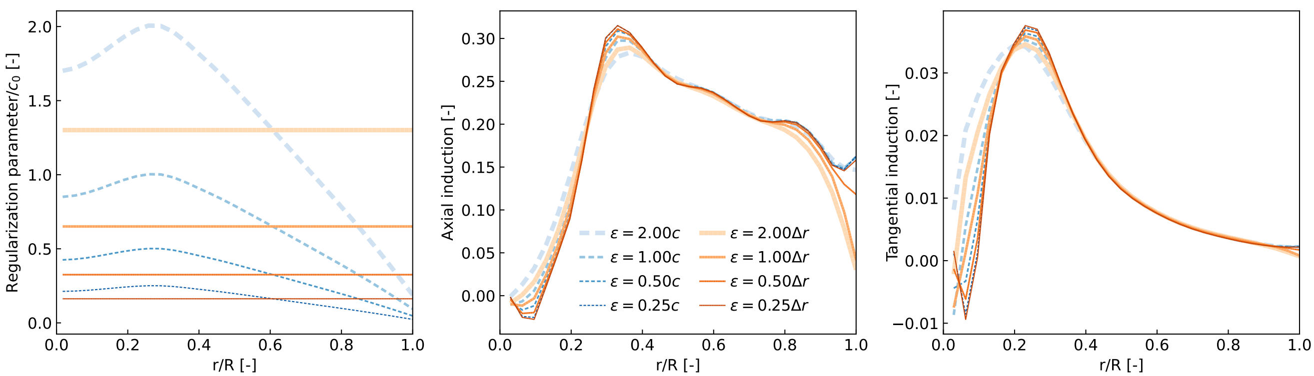

Figure 4. Influence of the regularization parameter on the induction factors obtained along a wind turbine blade. Left: regularization parameter normalized by maximum chord. Center: axial induction. Right: tangential induction.

3.2.3 Discussion on regularization

We observed a strong dependence of the flow quantities on the lifting line with respect to the regularization parameter. We expect that the regularization parameter should be characteristic of the physical size of the bound vorticity to obtain a realistic simulation of a wing or a turbine blade. This physical size is ~~expected to be~~ related to the size of the boundary layer~~and the spanwise discretization (Branlard, 2017). The impact~~ (Branlard, 2017), which is often proportional to the chord. As we observed, results will also be a function of the spanwise discretization. Vortex methods require the size of the regularization ~~is clearly observed on , and the choice of the regularization parameter can have a drastic impact on the results.~~ parameter to be proportional to the grid size for the method to converge to the Euler or Navier-Stokes equations (Cottet and Koumoutsakos, 2000)

. Therefore, physical and numerical regularizations operate differently, and we expect that a reformulation of the lifting-line algorithm itself is necessary to ensure convergence of the method. Additionally, vortex methods introduce more scales as the temporal and spatial discretization is refined. The regularization in the wake is essential to filter some of these new scales introduced. An adequate and physical filtering may be achieved using subgrid scale models and proper account of viscous diffusion—but such models are not readily available for a filament-based vortex method and are hard to achieve unless the topology and connectivity of the wake are modified. The topic of regularization is being actively researched ~~(Martínez-Tossas and Meneveau, 2019; Meyer Forsting et al., 2019; Li et al., 2020).~~ for actuator line CFD (Martínez-Tossas and Menevea and vortex-based methods (Li et al., 2020). Future work should focus on the convergence of the lifting-line method with blade discretization, and convergence of the filament-based vortex method, through comparisons with measurements and blade-resolved simulations.

3.2.4 ~~HAWT~~

3.3 HAWT—Comparison with BEM

AeroDyn was previously dedicated to ~~HAWT~~ HAWTs, and its BEM implementation was extensively tested for such configurations. In this section, we present comparisons between BEM, OLAF, and measurements for the 3-bladed NEG-Micon NM80 turbine, rated at $2\ \mathrm{MW}$, with a rotor diameter of $80\ \mathrm{m}$. Details about the turbine and the experimental setup ~~is found~~ are available in the DanAero report (Madsen et al., 2010). We use the test cases from the International Energy Agency (IEA) Wind Task 29 as validation cases (Schepers et al., 2021). In this work, we present results using the AeroDyn driver for a rigid rotor. Results using OpenFAST for a flexible rotor are ~~given~~ provided in the IEA Wind Task 29 report, together with a full description of the IEA Wind Task 29 test cases and results from other participants. For the cases presented below, flexibility effects were found to have a negligible ~~impacts on the~~ impact on results.

3.3.1 Uniform inflow

We begin with case IV.1.2 from the IEA Wind Task 29. The rotor operates at a tip-speed ratio of $\lambda = 8.5$ for an average wind speed of $U_0 = 6.1\ \mathrm{m/s}$. The test case neglects shear, and constant uniform inflow is assumed for the simulations. The force coefficients normal and tangential to the chord line are shown in Figure 5. The coefficients were obtained by normalizing the forces with $1/2\pi\rho U_0^2 R$, ~~with~~ where R is the rotor radius ~~,~~ and ρ is the air density. The simulation results shown in Figure 5 are consistent with results obtained by other institutions (~~see~~ Schepers et al. (2021)), both for the BEM and vortex code. The comparison with measurements is fair, but leaves room for improvement. ~~The differences are primarily attributed to the definition of the polar data used by the lifting line codes, which needs to be improved in the follow-up task (Schepers et al., 2021)~~ We discuss these results further in 3.3.3.

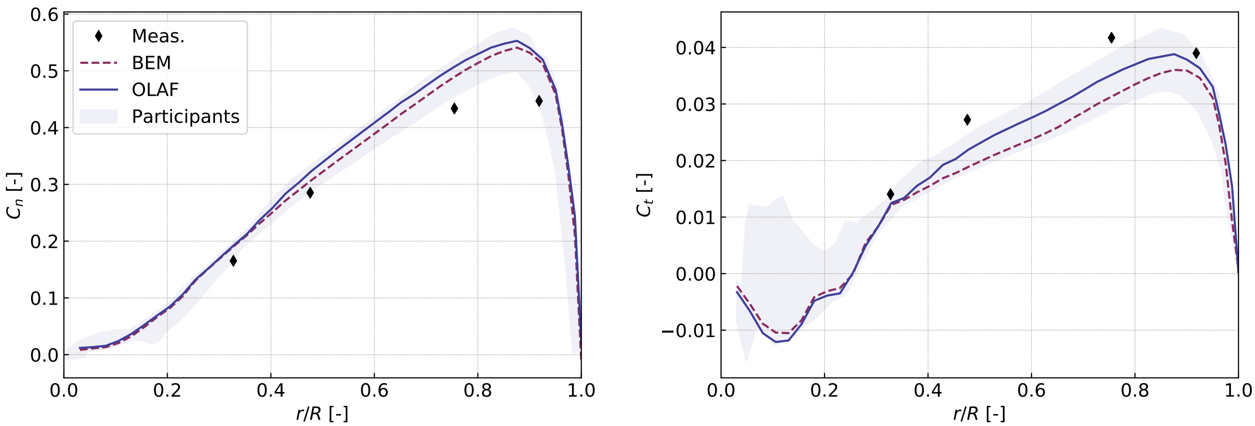

Figure 5. Simulation of a ~~horizontal axis wind turbine~~ HAWT using the AeroDyn driver. Results for test case IV.1.2 (constant, uniform inflow) of IEA Task 29. Normal and tangential force coefficients along the blade span (~~resp.~~ respectively, left and right).

3.3.2 Sheared and yawed inflow

We use cases IV.2.1 and IV.2.2 to study the aerodynamics in sheared and yawed conditions, respectively. Both cases have the same rotational speed and pitch~~,~~; the tip-speed ratios are 6.9 and 8.0, respectively; the yaw angles ~~,~~are 6° and 38~~°deg~~°, respectively; and the power law exponents ~~,~~are 0.25 and 0.26~~respectively.~~, respectively. We model the tower shadow effect using the potential flow model of OpenFAST. Figure 6 presents the results for both cases as a function of the azimuthal position. ~~The~~ We interpolated the normal loads and tangential loads ~~are shown as function of the azimuth, at four radial positions~~ radially to obtain them at the radial positions of the measurements: $r/R = [0.33, 0.48, 0.75, 0.92]$. The azimuth is 0 when the blade is pointing up~~. Both~~, and 180 when passing the tower, where the tower shadow model effect is visible. We performed elastic (with ElastoDyn) and rigid (with AeroDyn driver) simulations~~were performed. Some differences are observed~~. We observe some differences between the two (comparing dashed and plain lines of the same color) but these differences are not as pronounced as the differences between ~~the~~ BEM and OLAF (comparing blue and red curves). The vortex code agrees significantly better with the measurements than the BEM method for the yawed case. The shear-only case appears to be challenging, especially ~~towards the root. The~~ at 33% and 48% span, where the behavior captured by the codes is opposite to what is observed in the measurements.

3.3.3 Discussion on the results

Despite the simplicity of the uniform inflow case, we observed some differences between the BEM and vortex methods in the results presented in Figure 5. The differences are attributed to the fact that the rotor is at a moderately high load as well as to fundamental differences in the formulation. BEM assumes the blade annuli to be independent, does not inherently account for out-of-plane effects such as prebend, and relies on empirical corrections. In this simulation, the average induction factor is 0.4, corresponding to a moderately high loading case where a high-thrust correction is needed in BEM. Segment-based vortex

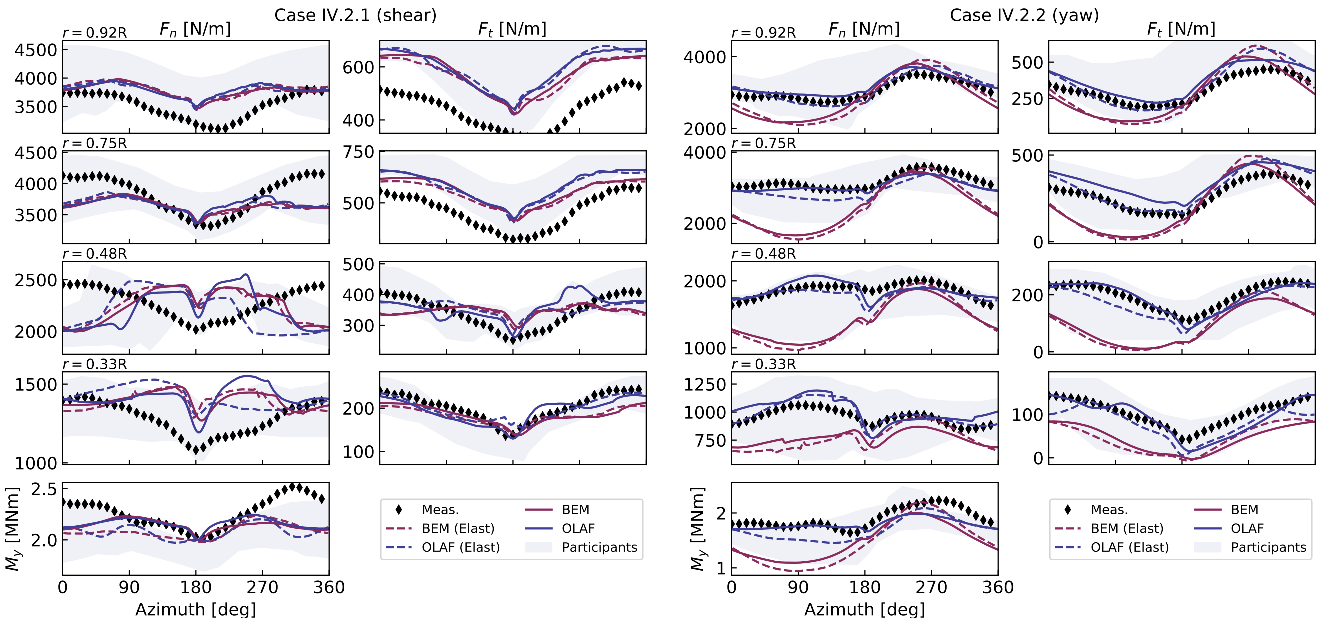

Figure 6. Results for a ~~horizontal axis wind turbine~~ HAWT (NM 80) under strong shear (left) and yawed (right) conditions. The normal (F_n) and tangential (F_t) loads are shown at four radial positions as a function of the azimuth. The blade root flapping moment, M_y, is shown at the bottom. Elastic ("Elast") and rigid simulations are compared to the DanAero measurements.

methods are of higher-level fidelity, but they suffer from the issue of regularization mentioned in 3.2. The mean relative errors in axial inductions and angle of attack are 4% between the two methods. The mean relative error of the tangential induction is around 20%, and the error in normal and tangential forces is 3% and 6%, respectively. The differences between BEM and vortex methods are in line with results from other participants.

The discrepancies between BEM and OLAF observed in the yaw case (Figure 6) indicate that the implementation of the yaw model in AeroDyn may need further improvements. It is possible that BEM implementation changes, such as those presented by Branlard et al. (2014) or Perez-Becker et al. (2020), could improve the results. Nevertheless, reasons for such discrepancies will require further investigation.

3.3.4 ~~Discussion on the results~~

The differences observed between measurements and simulations in Figure 5 and Figure 6 were primarily attributed to the definition of the polar data used by the lifting-line codes in the IEA report (Schepers et al., 2021). In general, the CFD-based method performed better than the lifting-line methods. Therefore, we expect an improvement of results using an updated set of polars.

3.4 VAWT

3.4.1 2D case

In this section, we use the 2D ~~vertical axis wind turbine (VAWT)~~ VAWT model presented by ~~Ferreira et al.(Ferreira et al., 2014)~~ Ferreira et al. (2014): a two-bladed turbine of radius $R = 1$ m, with blades of constant chord $c = 0.1$ m, and 15% relative thickness. The lift coefficient is set to $C_l = 2\pi 1.11 \sin\alpha$, and the drag and moment coefficients are zero. The tip-speed ratio is $\lambda = 4.5$. Simulations were run using the vortex code CACTUS (Murray and Barone, 2011), and with OLAF, and compared with double multiple ~~stream tube~~ streamtube model (DMST) ~~from (Ferreira et al., 2014)~~results that we extracted from the figure of Ferreira et al. (2014). The angle of attack as a function of azimuth is shown in Figure 7. The ~~vortex~~ differences between the vortex code results and the DMST are similar to what was observed and discussed by Ferreira et al. The vortex codes CACTUS and OLAF are observed to strongly agree in this case for the estimation of the angle of attack. CACTUS uses a vortex formulation where the velocity at control points is obtained from the average of the velocity at the nodes, and where the wake is being shed at the ~~lifting-line~~lifting line. The original OLAF formulation uses the induced velocity obtained in between nodes and sheds the wake at the trailing edge of the blade. For this work, OLAF was modified ~~so as to be able to~~ to have a similar formulation as CACTUS. In the case presented in Figure 7, ~~it is seen~~ we observe that by using the same formulation (i.e., comparing CACTUS and OLAF “CP+Wake“ on the figure), a slightly better agreement is obtained. A more significant impact of the implementation was observed on other simulations. ~~The choice of implementation of~~ Some authors argue that unsteady effects are better captured when the shedding of vorticity occurs at the trailing edge or a quarter chord behind the trailing edge (Katz and Plotkin, 2001). Such conclusions are likely to be true for panel methods but might not apply

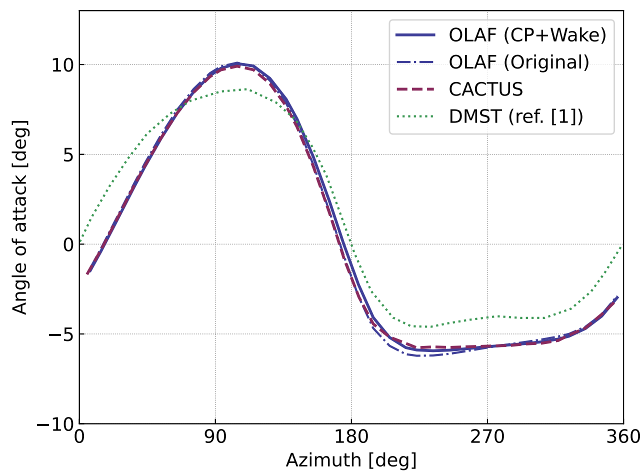

Figure 7. Angle of attack on a 2D VAWT as obtained with various vortex methods and with the double multiple ~~stream tube~~ streamtube (DMST) theory.

for lifting-line vortex methodsmethods. In light of the current results, it appears that this choice of implementation for VAWTs (shedding at trailing edge, location of control points) remains may still be an open question.

The previous test case doesn't activate the dynamic stall model[2] as a results result of the low angle of attack and artificial lift-coefficient lift coefficient used. We replaced the polar data with a realistic polar data of a NACA0015 airfoil which that stalls at approximately 8.5 deg. The angle of attack is similar to the one obtained in Figure 7, oscillating between ± 10 deg., but the dynamic stall has a strong influence on the lift coefficient and power coefficient. In this work, we implemented the Boeing-Vertol (BV) model , BV model and the dynamic stall model of Øye. AeroDyn also includes three variations of the Beddoes-Lesihman Beddoes-Leishman (BL) model (Leishman and Beddoes, 1989): the Gonzalez 's (BL Gonz.) and the Minemma/Pierce (BL MP) variants (Damiani and Hayman, 2019), and the 4-states model from Hansen et al. (Hansen et al., 2004) (BL HGM). The impact of the choice of the dynamic stall on the power coefficient is shown in Figure 8 for a simulation at $\lambda = 4.5$. From the figure, it is observed that the choice of dynamic stall model has a dramatic impact on the aerodynamic

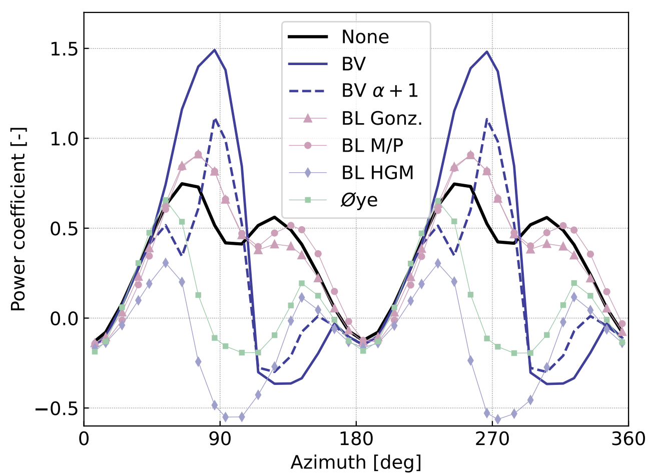

Figure 8. Influence of the choice of dynamic stall model on the power coefficient of a 2D vertical axis wind turbineVAWT.

performancesperformance. It is common practice in the VAWT VAWTs community to tune the parameters of the dynamic stall model such as to achieve performances that matches match the measurements. To illustrate this, we increased the stall angle parameter of the Boeing-Vertol BV model by 1 deg (labeled as "BV $\alpha + 1$" on the figure). Again, such a change has a strong impact on the response, delaying the onset and activation of the dynamic model. It is clear how such tuning of the coefficients can lead to desired responses and performances. Overall, the spread of results indicates that dynamic stall models for VAWT (andlikely HAWTVAWTs (and, likely, HAWTs) should be the topic of future research.

[2] In this article, we use the term "dynamic stall" to refer to unsteady aerodynamics effects on an airfoil section (including unsteady attached flows).

3.4.2 3D case—Comparison with measurements

In this section, we model a prototype 5-kW VAWT with the new AeroDyn driver. The turbine consists of 9 ~~blades: 3~~ blades—3 vertical blades, each attached to the hub by ~~two~~ 2 support arms. A picture of the wind turbine is shown in Figure 9. The turbine was designed and constructed by XFlow Energy and was tested at the Field Laboratory for Optimized Wind Energy (FLOWE) in Lancaster, ~~CA~~California. The turbine was tested between February and April 2020. The field measurements were

Figure 9. ~~Photo of~~ XFlow's 5-kW prototype VAWT at the Field Laboratory for Optimized Wind Energy in Lancaster, ~~CA~~California.

collected using two 6-axis load cells mounted between the vertical blades and its support arms. The load cells were custom units developed by Sensing Systems from Dartmouth, ~~MA~~Massachusetts. The wind speed was measured using a pair of APRS #40R anemometers, positioned 2 rotor diameters upstream of the rotor. The measurements presented have had inertial effects subtracted.

First, we run simulations with steady inflow and constant rotational speed to ~~evaluated~~ evaluate the power curve of the turbine. The power coefficient as a function of tip-speed ratio ~~are~~ is compared to field measurements in Figure 10. ~~For both vortex codes, the power coefficient was corrected to account for excrescences as follows:~~ We used two different sets of inputs for these simulations: the first one favors CACTUS, whereas the second set favors OLAF. In the first set, the dynamic stall coefficients of the BV model were tuned such that the CACTUS simulation would match the measured power curve, and the

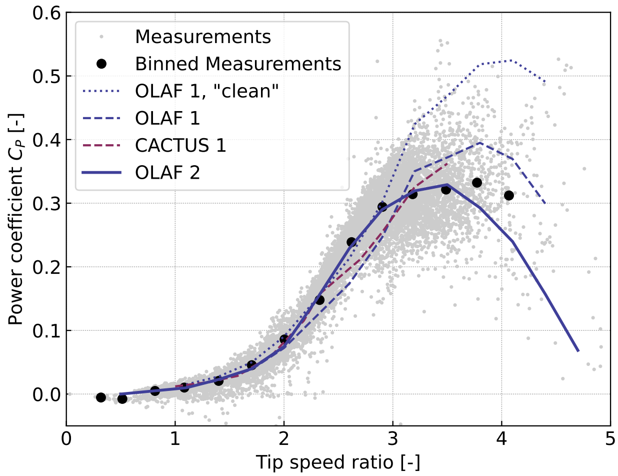

Figure 10. Performance of the VAWT model as obtained with the simulation tools OLAF and CACTUS~~and~~, compared with measurements for two sets of inputs (one tuned for CACTUS, another tuned for OLAF). The curve "OLAF ~~(~~1, clean~~)~~" does not include excrescences.

excrescences (drag losses associated with connections, bolts, etc.) were computed as an additional loss term:

$$C_P = C_{P,\text{clean}} - \Omega \frac{[C_{Q,\text{exc}} 1/2\rho(R^2)R(\Omega R)^2]}{1/2\rho(2R^2)U_0^3} \frac{[C_{Q,\text{exc}} 1/2\rho(R^2)R(\Omega R)^2]}{1/2\rho(2R)^2U_0^3} \tag{1}$$

where $C_{P,\text{clean}}$ is the power coefficient obtained from the vortex code with clean polars, and the term in ~~bracket~~ brackets is the excrescences torque, which is further defined in (Murray and Barone, 2011). The excrescences torque coefficient was evaluated ~~experimentally to $C_{Q,\text{exc.}} = 0.009$.~~ by computing the difference between the experimental and CACTUS-simulated torque for a case where the turbine rotation is prescribed but the inflow is zero, giving $C_{Q,\text{exc}} = 0.009$. In the second method, we performed a joint optimization of the drag polars and the dynamic stall parameters such that the OLAF results would match the power curve measured in the field. In this second case, the excrescences were directly accounted for by the increased drag in the polar data, which was expected to be more realistic. In Figure 10, the results labeled "OLAF ~~(clean)~~1, clean" are results from the first set of inputs, without the excrescences ~~, whereas the label "OLAF" and "CACTUS" include the excrescences. We observed~~ and with the clean polars. The labels "1" or "2" indicate which sets of input are used. We observe in Figure 10 that both vortex codes capture the main characteristics of the power curve.

Despite a similar implementation used between OLAF and CACTUS, some differences of outputs for this advanced structure are observed. ~~The~~ For the first set of results (tuned for CACTUS), the performances obtained using OLAF appear to be ~~under predicted~~ under-predicted below $\lambda = 3$ and ~~over predicting otherwise. It is noted that the dynamic stall coefficients of the Boeing-Vertol model were tuned such that the CACTUS simulation would match the measured power curve . It is expected that another~~ over-predicted otherwise, indicating that the difference in implementation can have an important impact on the predictions. The second set of results shows that OLAF can capture the experimental power curve using a different tuning of the dynamic stall coefficients~~for OLAF would lead to stronger agreement with the measurements.~~ . This second set of results also illustrates that a tuning of the drag coefficient is possible to account for excrescences instead of adding a constant torque.

We illustrate the differences between the models by looking at time traces of the total force on the first vertical blade at different tip-speed ratios. Dimensionless force coefficients are computed as $C = F/(1/2\rho(2R)^2U_0^2)$, where F is the force in a given direction. The forces are reported in the coordinate of the blade ~~as illustrated~~ (described in Figure 1). The force coefficients obtained from field measurements and simulation are compared in Figure 11. To demonstrate the capabilities of the AeroDyn driver, simulations with shear and turbulence were also carried ~~on~~out. The power law profiles and turbulence intensities from the field measurements were used to generate synthetic turbulent inflow with TurbSim (Jonkman and Buhl, 2006). Results from these simulations, averaged over 24 revolutions, are indicated by the label “OLAF (turb)” on ~~figure~~ Figure 11. The azimuthal positions 90° and 270° correspond to the ~~position~~ positions where the blade is upwind and downwind,

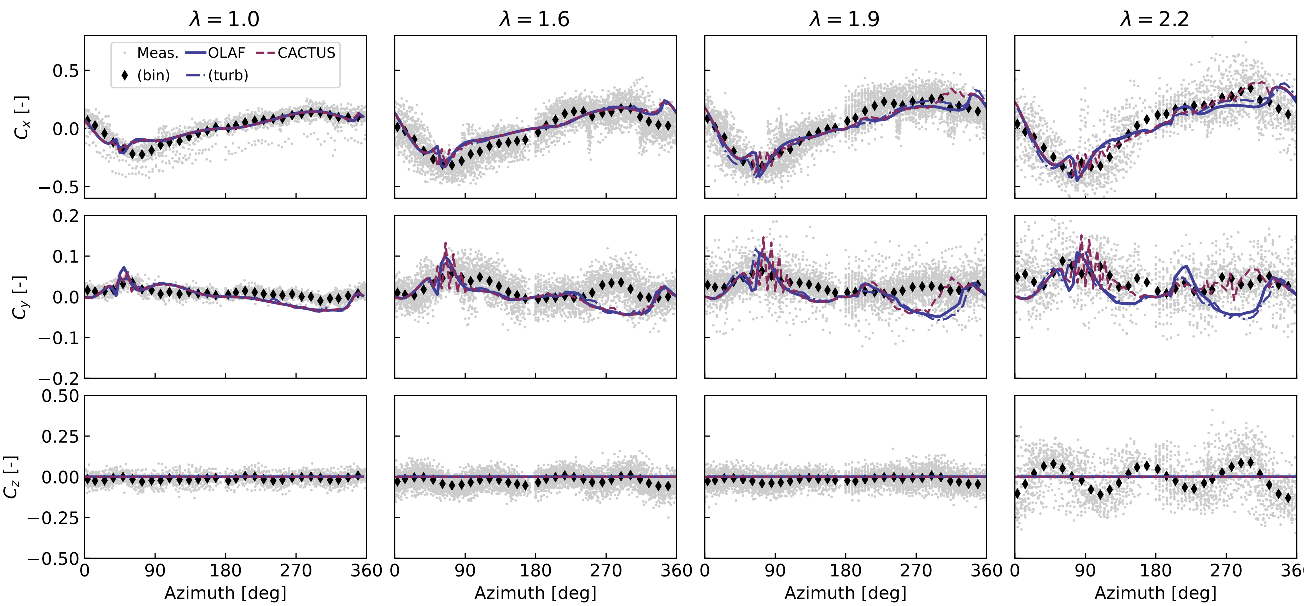

Figure 11. Force coefficients as measured and simulated on the ~~vertical axis turbine~~ VAWT model.

respectively. A fair agreement with the measurements is obtained for both tools. The response when the blade is in the wake (270°) ~~appear~~ appears more challenging to capture, in particular at higher tip-speed ratios and for the tangential coefficient (C_y). This likely ~~indicate~~ indicates issues related to the estimation of the drag force or the account of viscous effects in the wake. In general, a strong agreement is observed between OLAF and CACTUS. Spikes observed in the CACTUS simulations are not present in the OLAF runs, which displays a smoother response. The differences between the turbulent and uniform simulations appear to be minor ~~for these cases~~ but are expected to become more important for larger shear and turbulence intensities.

Based on a finite element analysis of XFlow's ~~5-~~5 kW turbine geometry, we expect C_x to be the least affected by ~~aero-elastic~~ aeroelastic effects. This agrees well with the simulation ~~,~~and is a possible explanation for discrepancies ~~between~~ observed in the simulated C_y and C_z ~~from the field and simulation~~compared to the field results. Based on the finite element analyses, the turbine's first mode of excitation corresponds to a vertical motion of the blades, which is observed to be a dominant effect in the field measurements. Because of this, it is not surprising that the rigid-body AeroDyn/OLAF simulations did not capture the oscillations observed in C_z. Future work coupling OLAF with an elastic solver should more accurately capture this effect.

3.5 Discussions on vertical axis simulations with vortex methods

In this section, we presented examples of simulations of 2D and 3D VAWTs, verified them using other simulation tools, and validated them against measurements.

By diving into the implementation details of CACTUS, we found some differences of formulation, which can explain the differences observed between the two simulation codes. Some of the differences between OLAF and CACTUS include: the presence (or absence) of a "trailing-edge" vortex, the location of the control points (on the nodes or in between them), and the location of the points used for the determination of the angle of attack (CACTUS uses points at the 1/4, 1/2, and 3/4 chord for the BV model). Additional features were implemented in OLAF and it is now possible to switch between these formulations. Additional work is needed to determine which formulation is the most accurate.

The current approach for VAWTs modelers consists of tuning the dynamic stall parameters to obtain performances that match the measured ones. We applied this approach in this work to illustrate that the method can indeed be used successfully. Nevertheless, the approach cannot be considered satisfactory, and the large spread of results that we obtained in Figure 8 for different dynamic stall models indicates that more research is needed on the topic. In particular, future work should focus on deep stall and large fluctuations of angle of attack, which are relevant for VAWTs.

We found that when the turbine passes its own wake, the simulated loads were in noticeable discrepancy with the field measurements. The reasons for such differences are currently not well understood. They may be related to regularization issues and, potentially, the lack of vorticity shedding when the blade is stalling. It is also possible that the blade-vortex interaction is not well captured by the lifting-line vortex method. Flow field measurements focusing on the wake and its interaction with the blade may help answer this question.

4 Conclusions

In this work, we described the features of a general-purpose driver to perform aerodynamic simulations of wind energy concepts. ~~Different applications were presented~~ We demonstrated different applications to highlight the versatility of the ~~driver and point to areas of~~ new driver. In most applications, we used the vortex code OLAF, and we presented verifications and validations of this newly implemented code. Throughout the article, we pointed to different areas for future research, namely:

– ~~The~~ We showed that the regularization parameter of lifting-line vortex methods, commonly referred to as the "vortex core," has a strong impact on the accuracy of the ~~results,~~ lifting-line quantities and should be further investigated. Measurement and blade-resolved CFD can be used as a reference, providing detailed load distributions along the blades and flow fields of the wake. The lifting-line method should be improved to ensure convergence as the spanwise discretization is increased, while preserving a physical size of the regularization parameter and, therefore, ensuring that physical flow fields are obtained near the blade and in the wake. Filament-based vortex methods should also display convergence in the wake for increased spanwise and temporal resolutions. Such convergence might require the implementation of dedicated viscous and subgrid scale models.

- ~~Different~~ We found that different lifting-line vortex code implementations can lead to different loads and induction field, depending on the choice of formulation. Some of the differences between OLAF and CACTUS include: the presence (or absence) of a "trailing-edge" vortex, the location of the control points (on the nodes or in between them), and the angles of attack used in dynamic stall models. Some of CACTUS formulations were implemented in OLAF. Additional work is needed to determine which formulation is the most accurate.

- ~~The blade element momentum~~ Using the IEA Task 26 test cases, we observed that the BEM theory is challenged by out-of-plane situations (yaw, shear, and coning) ~~,~~ and, despite the ad-hoc corrections available, the method does not capture all the trends observed in measurements. Using OLAF showed a substantial improvement in the yawed test case; therefore, future work will be dedicated to improving the yaw model of AeroDyn.

- The choice of dynamic stall model significantly impacts the simulation results of ~~VAWT, and practitioners~~ VAWTs. Practitioners commonly fall back to tuning the parameters of the model ~~, in lack of~~ because we lack a universal and reliable model. More research is needed on the topic; specifically, focusing on deep stall and large fluctuations of angle of attack, which are relevant for VAWTs.

- We noted that for VAWTs, the differences between measured and simulated loads were noticeable when the blade passes in the wake. We hypothesized that this could be due to a poor capture of the blade-vortex interaction, or a flawed representation of the wake due to nonphysical regularization, or due to a lack of vorticity shedding when the profiles are in stall.

Aerodynamic concepts different from the widely studied ~~horizontal axis turbines,~~ HAWTs offer a variety of aerodynamic challenges. The new aerodynamic driver opens the door for further investigation of these concepts. Targeted aerodynamic studies within a controlled environment can be carried ~~on~~ out using the new prescribed motion feature. The feature is relevant for future aerodynamic research areas, including ~~:~~ floating offshore wind turbines or unsteady aerodynamics effects under (prescribed) elastic motions (e.g., flutter). The aerodynamic models currently implemented in AeroDyn ~~consists of the Blade Element Momentum~~ consist of the BEM method (both quasi-steady and dynamic) and a lifting-line vortex lattice solver. AeroDyn will soon be extended to support ~~hydro-kinetic~~ hydrokinetic turbines. Additional models will ~~also~~ be added in the future, such as the double multiple streamtube model ~~,~~ and mixed formulations between BEM and vortex methods.

References

Alvarez, E. J. and Ning, A.: Modeling Multirotor Aerodynamic Interactions Through the Vortex Particle Method, in: AIAA Aviation Forum, Dallas, TX, https://doi.org/10.2514/6.2019-2827, 2019.

Bangga, G., Dessoky, A., Wu, Z., Rogowski, K., and Hansen, M. O.: Accuracy and consistency of CFD and engineering models for simulating vertical axis wind turbine loads, Energy, 206, https://doi.org/10.1016/j.energy.2020.118, 2020.

Boorsma, K., Wenz, F., Lindenburg, K., Aman, M., and Kloosterman, M.: Validation and accommodation of vortex wake codes for wind turbine design load calculations, Wind Energy Science, 5, 699–719, 2020.

Bortolotti, P., Johnson, N., Abbas, N. J., Anderson, E., Camarena, E., and Paquette, J.: Land-Based Wind Turbines with Flexible Rail-Transportable Blades — Part 1: Conceptual Design and Aeroservoelastic Performance, Wind Energy Science, 6, 1277–1290, https://doi.org/10.5194/wes-6-1277-2021, 2021.

Branlard, E.: Wind Turbine Aerodynamics and Vorticity-Based Methods: Fundamentals and Recent Applications, Springer International Publishing, https://doi.org/10.1007/978-3-319-55164-7, 2017.

Branlard, E., Gaunaa, M., and Machefaux, E.: Investigation of a new model accounting for rotors of finite tip-speed ratio in yaw or tilt, Journal of Physics: Conference Series (Online), 524, 1–11, https://doi.org/10.1088/1742-6596/524/1/012124, 2014.

Branlard, E., Papadakis, G., Gaunaa, M., Winckelmans, G., and Larsen, T. J.: Aeroelastic large eddy simulations using vortex methods: unfrozen turbulent and sheared inflow, Journal of Physics: Conference Series (Online), 625, https://doi.org/10.1088/1742-6596/625/1/012019, 2015.

Chatelain, P., Backaert, S., Winckelmans, G., and Kern, S.: Large Eddy Simulation of Wind Turbine Wakes, Flow Turbulence and Combustion, 91, 587–605, https://doi.org/10.1007/s10494-013-9474-8, 2013.

Cottet, G.-H. and Koumoutsakos, P.: Vortex methods: theory and practice, Cambridge University Press, 2000.

Damiani, R. and Hayman, G.: The Unsteady Aerodynamics Module for FAST 8, Tech. Rep. NREL/TP-5000-66347, National Renewable Energy Laboratory, 2019.

De Vries, O.: Fluid dynamic aspects of wind energy conversion, AGARD report, Brussels, Belgium, AG-243, 1–50, 1979.

Ferreira, C. S., Madsen, H. A., Barone, M., Roscher, B., Deglaire, P., and Arduin, I.: Comparison of aerodynamic models for Vertical Axis Wind Turbines, Journal of Physics: Conference Series, 524, https://doi.org/10.1088/1742-6596/524/1/012125, 2014.

Folkersma, M., Schmehl, R., and Viré, A.: Fluid-Structure Interaction Simulations on Kites, in: Airborne Wind Energy Conference 2017, AWEC 2017; Conference date: 05-10-2017 through 06-10-2017, pp. 144–144, https://doi.org/10.4233/uuid:4c361ef1-d2d2-4d14-9868-16541f60edc7, 2017.

Glauert, H.: Airplane propellers, Division L, in: Aerodynamic Theory, Volume IV, edited by W. F. Durand, Julius Springer, Berlin, 1935.

Grasso, F., van Garrel, A., and Schepers, G.: Development and Validation of Generalized Lifting Line Based Code for Wind Turbine Aerodynamics, Tech. Rep. ECN-M–11-004, ECN, 2011.

Hansen, M., Gaunaa, M., and Aagaard Madsen, H.: A Beddoes-Leishman type dynamic stall model in state-space and indicial formulations, Tech. rep., Risø National Laboratory, Roskilde, Denmark, 2004.

Jonkman, B. and Buhl, M.: TurbSim User's Guide, Tech. Rep. NREL/TP-500-39797, National Renewable Energy Laboratory, 2006.

Jonkman, J.: Makani Energy Kite Modeling - Cooperative Research and Development Final Report, Tech. Rep. NREL/TP-5000-80635, National Renewable Energy Laboratory, 2021.

Katz, J. and Plotkin, A.: Low-Speed Aerodynamics, 2nd Edition, Cambridge Aerospace Series (No. 13), Cambridge University Press, 2001.

Leishman, J. G. and Beddoes, T.: A semi-empirical model for dynamic stall, Journal of the American Helicopter Society, 34, 3–17, 1989.

Li, A., Gaunaa, M., Pirrung, G. R., Ramos-García, N., and Horcas, S. G.: The influence of the bound vortex on the aerodynamics of curved wind turbine blades, Journal of Physics: Conference Series, 1618, 052 038, https://doi.org/10.1088/1742-6596/1618/5/052038, 2020.

Madsen, H. A., Bak, C., Paulsen, U. S., Gaunaa, M., Fuglsang, P., Romblad, J., Olesen, N. A., Enevoldsen, P., Laursen, J., and Jensen, L.: The DAN-AERO MW Experiments - Final Report, Tech. Rep. Riso-R-1726, Risø-DTU, 2010.

Makridis, A. and Chick, J.: Validation of a CFD model of wind turbine wakes with terrain effects, Journal of Wind Engineering and Industrial Aerodynamics, 123, 12–29, https://doi.org/https://doi.org/10.1016/j.jweia.2013.08.009, 2013.

Marten, D., Wendler, J., Pechlivanoglou, G., Nayeri, C., and Paschereit, C.: QBlade: an open source tool for design and simulation of horizontal and vertical axis wind turbines, International Journal of Emerging Technology and Advanced Engineering, 3, 264–269, 2013.

Martínez-Tossas, L. A. and Meneveau, C.: Filtered lifting line theory and application to the actuator line model, Journal of Fluid Mechanics, 863, 269–292, https://doi.org/10.1017/jfm.2018.994, 2019.

Meyer Forsting, A. R., Pirrung, G. R., and Ramos-García, N.: A vortex-based tip/smearing correction for the actuator line, Wind Energy Science, 4, 369–383, https://doi.org/10.5194/wes-4-369-2019, 2019.

Moriarty, P. J. and Hansen, A. C.: AeroDyn Theory Manual, Tech. Rep. NREL/EL-500-36881, National Renewable Energy Laboratory, 2005.

Murray, J. and Barone, M.: The development of CACTUS: a wind and marine turbine performance simulation code., in: 49th AIAA Aerospace Sciences Meeting, Orlando, Florida, 2011.

OpenFAST: Open-source wind turbine simulation tool, available at http://github.com/OpenFAST/OpenFAST/, 2021.

Øye, S.: Dynamic stall, simulated as a time lag of separation, Proceedings of the 4th IEA Symposium on the Aerodynamics of Wind Turbines, 1991.

Paraschivoiu, I. and Delclaux, F.: Double multiple streamtube model with recent improvements (for predicting aerodynamic loads and performance of Darrieus vertical axis wind turbines), Journal of Energy, 7, 250–255, https://doi.org/10.2514/3.48077, 1983.

Perez-Becker, S., Papi, F., Saverin, J., Marten, D., Bianchini, A., and Paschereit, C. O.: Is the Blade Element Momentum theory overestimating wind turbine loads? – An aeroelastic comparison between OpenFAST's AeroDyn and QBlade's Lifting-Line Free Vortex Wake method, Wind Energy Science, 5, 721–743, https://doi.org/10.5194/wes-5-721-2020, 2020.

Rezaeiha, A., Kalkman, I., and Blocken, B.: CFD simulation of a vertical axis wind turbine operating at a moderate tip speed ratio: Guidelines for minimum domain size and azimuthal increment, Renewable Energy, 107, 373–385, https://doi.org/https://doi.org/10.1016/j.renene.2017.02.006, 2017.

Saverin, J., Marten, D., Pechlivanoglou, G., and Paschereit, C.: Advanced Medium-Order Modelling of a Wind Turbine Wake with a Vortex Particle Method Integrated within a Multilevel Code, Journal of Physics: Conference Series, 1037, 062 029, https://doi.org/10.1088/1742-6596/1037/6/062029, 2018a.

Saverin, J., Persico, G., Marten, D., Holst, D., Pechlivanoglou, G., Paschereit, C., and Dossena, V.: Comparison of Experimental and Numerically Predicted Three Dimensional Wake Behavior of Vertical Axis Wind Turbines, Journal of Engineering for Gas Turbines and Power, https://doi.org/10.1115/1.4039935, 2018b.

Schepers, J., Boorsma, K., Madsen, H., Pirrung, G., Bangga, G., Guma, G., Lutz, T., Potentier, T., Braud, C., Guilmineau, E., Croce, A., Cacciola, S., Schaffarczyk, A. P., Lobo, B. A., Ivanell, S., Asmuth, H., Bertagnolio, F., Sørensen, N., Shen, W. Z., Grinderslev, C., Forsting, A. M., Blondel, F., Bozonnet, P., Boisard, R., Yassin, K., ¨oning, L. H., , Stoevesandt, B., Imiela, M., Greco, L., Testa, C., Magionesi, F., Vijayakumar, G., Ananthan, S., Sprague, M. A., Branlard, E., Jonkman, J., Carrion, M., Parkinson, S., and Cicirello, E.: Final report of Task 29, Phase IV: Detailed Aerodynamics of Wind Turbines, Tech. rep., IEA Wind, Task 29, 2021.

Shaler, K., Branlard, E., and Platt, A.: OLAF User's Guide and Theory Manual, Tech. Rep. NREL/RP-5000-75959, National Renewable Energy Laboratory, 2020.

Sørensen, N. N.: General purpose flow solver applied to flow over hills, Ph.D. thesis, Risø-DTU, 1995.

Sprague, M., Ananthan, S., Vijayakumar, G., and Robinson, M.: ExaWind: A multifidelity modeling and simulation environment for wind energy, Journal of Physics: Conference Series, 1452, 012 071, https://doi.org/10.1088/1742-6596/1452/1/012071, 2020.

Strickland, J.: The Darrieus Turbine: A Performance Prediction Model Using Multiple Stream tubes, Tech. Rep. SAND75-041, Sandia National Laboratories, 1975.

van Garrel, A.: Development of a wind turbine aerodynamics simulation module, Tech. Rep. ECN-C–03-079, ECN, 2003.

Weihing, P., Letzgus, J., Bangga, G., Lutz, T., and Krämer, E.: Hybrid RANS/LES Capabilities of the Flow Solver FLOWer—Application to Flow Around Wind Turbines, in: Progress in Hybrid RANS-LES Modelling, edited by Hoarau, Y., Peng, S.-H., Schwamborn, D., and Revell, A., pp. 369–380, Springer International Publishing, Cham, 2018.